ACS OMEGA

Open Access

http://pubs.acs.org/journal/acsodf

Article

AI-Based Geometry Recognition for Evaluating the Feasibility of Intensified Reaction and Separation Systems

Yongbeom Shin, Minyong Lee, Jeongwoo Lee, Donggun Kim, and Jae W. Lee*

Cite This: *ACS Omega* 2023, 8, 48413−48431

Read Online

ACCESS | Metrics & More | Article Recommendations | Supporting Information

ABSTRACT: Reactive distillation (RD) provides notable advantages over conventional processes, regarding reduced energy requirements and CO_2 emissions. However, as the benefits of RD may not be universally applicable, a comprehensive feasibility assessment is necessary. This study introduced an automated feasibility evaluation procedure for an RD column using an AI-based region recognition approach, reducing the reliance on expert knowledge and heuristics in graphical methods. Through *k*-means clustering-based image segmentation, topological information on the reaction and separation reachable region was extracted from ternary diagram landscapes. Subsequently, the extracted information was integrated into tray-by-tray calculations to automate the evaluation. This geometric calculation procedure was applied to assess the feasibility of RD columns with different types of reactions. The feasibility results were obtained within seconds, demonstrating the efficiency of the proposed approach. Furthermore, case studies validated the feasibility of the evaluation results for three practical examples using rigorous simulations, confirming its reliability and applicability.

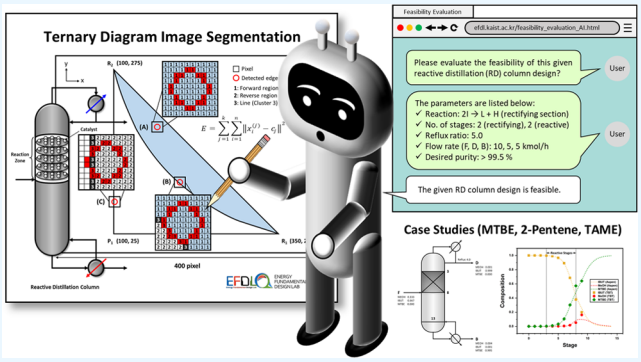

1. INTRODUCTION

10 to 15% of the global energy consumption is attributed to distillation techniques used for industrial separation.[1] Moreover, approximately 40% of the chemical industry's total energy consumption is from distillation processes, which is a significant portion of the energy used by the industry.[2,3] Industrial energy consumption continues to rely on fossil fuels, which contribute most of the CO_2 emissions.[4] Process intensification is considered an attractive solution for reducing the energy consumption of distillation processes through reduced equipment scale and efficiency outcomes.[5−7]

Reactive distillation (RD) is a promising intensification technique that integrates chemical reactions and separation into a single column filled with a catalyst, enabling the simultaneous removal of products and achieving high reaction conversion and yield by overcoming the equilibrium limit.[8,9] RD is an attractive approach for decreasing the energy consumption of distillation alone.[10] The practical applications of RD have demonstrated a significant reduction of 30 to 50% in capital costs and energy consumption compared to conventional processes with the risk of gas emissions mitigated.[11,12] The advantages of RD have led to numerous industrial implementations of etherification (e.g., methyl *tert*-butyl ether, ethyl *tert*-butyl ether, and *tert*-amyl methyl ether),[13,14] esterification (e.g., *n*-butyl acetate, *n*-amyl acetate, *n*-hexyl acetate, and cyclohexyl acetate),[15−17] transesterification (e.g., dimethyl carbonate, diethyl carbonate, and propylene glycol methyl ether acetate),[18−21] and olefin metathesis (e.g., 2-pentene) with a variety of studies conducted to improve the energy efficiency of the reaction and separation systems.[22] While RD offers significant advantages over conventional processes, it is important to note that its benefits may not always be applicable, which means an RD column is sometimes not beneficial in the infeasible integration of reaction and separation, and the reaction would impact the presence of separation boundaries.[23,24] Consequently, the feasibility of an RD column should be assessed under the given specifications to determine the suitability of implementing RD.

Various methods have been developed for the feasibility evaluation of RD systems, including graphical methods, optimization-based methods, and heuristic and evolutionary methods.[25] Graphical methods, which rely on topological information from residue curve maps (RCMs), are commonly used, because they provide an intuitive solution for determining the feasibility of chemical reactions occurring in an RD column, obtaining results with relatively fast and simple calculations.[25] In the literature, studies specifically address the feasibility evaluation of RD through graphical methods with

Received: October 16, 2023
Revised: November 15, 2023
Accepted: November 16, 2023
Published: December 5, 2023

https://doi.org/10.1021/acsomega.3c08128
ACS Omega 2023, 8, 48413−48431

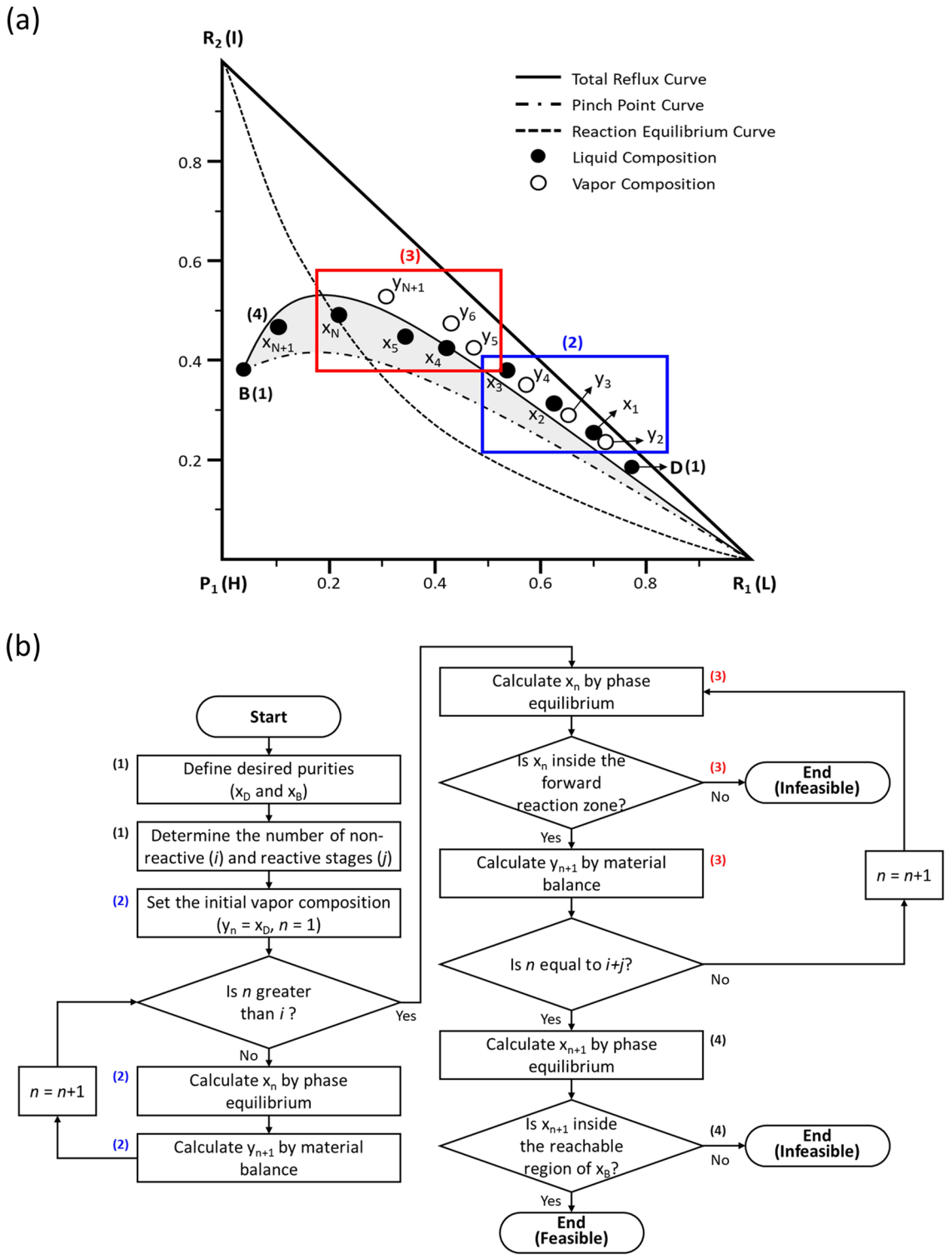

Figure 1. Graphical method for the feasibility evaluation of a reactive distillation column with a nonisomolar combination reaction, $L + I \leftrightarrow H$, in a rectifying section: (a) composition profiles on the ternary diagram and (b) flowchart for the feasibility evaluation procedure. R_1: reactant 1 (light), R_2: reactant 2 (intermediate), and P_1: product 1 (heavy).

the adaption of two traditional methods: the McCabe−Thiele and Ponchon−Savarit methods.[26−28] The practical applicability of the proposed method was validated by extending it to industrial processes, specifically the methyl *tert*-butyl ether (MTBE) and methyl acetate production systems.[29] Subsequently, various feasibility criteria have been proposed continuously for evaluating the feasibility of ternary systems,[30] complex quaternary,[31,32] quinary RD systems,[33] batch reactive distillation,[34] and a reactive dividing wall column.[35]

Nevertheless, since feasibility criteria are considered necessary conditions, the satisfaction of these criteria does not guarantee the feasibility of an RD column.[30] Therefore, systematic approaches are needed to evaluate the feasibility of a specific RD system beyond the criteria. A general algorithm

https://doi.org/10.1021/acsomega.3c08128
ACS Omega 2023, 8, 48413−48431

utilizing topological information was presented to evaluate the feasibility of a double-feed RD column and demonstrated with the example of *tert*-amyl methyl ether (TAME) that the algorithm enables the feasibility evaluation of quaternary reactive distillation systems without requiring rigorous stage calculations.[36] A shortcut method was proposed to accelerate the feasibility evaluation using the general algorithm by proposing a rapid composition profile generation approach for reactive and extractive distillation columns.[37] A feasibility evaluation algorithm for a complex batch reactive distillation column was introduced in a subsequent work.[38] Various frameworks for the feasibility evaluation of RD columns have been continuously reported in the literature.[39−43] However, the feasibility evaluation of an RD column still demands expert knowledge, and it is time-consuming due to the complexities of RD columns that arise from multiple interactions between vapor−liquid equilibrium and chemical kinetics.[44,45] Particularly, the extraction and interpretation of graphical information from ternary diagrams are necessary, which consists of determining the occurrence of the chemical reactions and ensuring the feasibility of crossing the distillation boundary and the desired purity of the products.

This study newly proposed an automated method for extracting and interpreting topological information from a ternary diagram and reaction equilibrium curve using the image segmentation method with *k*-means clustering, an unsupervised machine learning algorithm, to effectively evaluate the feasibility of RD columns for ternary systems. This approach enables feasibility evaluation without requiring expert knowledge and accelerates the procedure. First, this paper describes the feasibility evaluation of an RD column and the proposed automation method using image segmentation. Then, a feasibility evaluation of a single-feed column was performed based on the type of reaction (isomolar and nonisomolar), followed by a feasibility analysis of a double-feed column with a nonisomolar reaction. In addition, case studies were conducted on three systems, MTBE synthesis, 2-pentene metathesis, and TAME synthesis, to assess the proposed method by comparing it with rigorous simulation results using Aspen Plus V11.

2. AI-BASED GRAPHICAL FEASIBILITY EVALUATION METHOD

2.1. Feasibility Evaluation. A feasibility evaluation of an RD column was conducted based on the movement of the composition from the desired product on ternary diagrams.[30] Because the evaluation aims to assess the potential to overcome equilibrium limits such as azeotropes and distillation boundaries, the primary assumptions for the feasibility evaluation are as follows: (1) the heat of reaction is neglected, (2) the heat of vaporization is assumed to be constant, (3) the feed is assumed to be a saturated liquid, (4) the column is adiabatic, (5) all stages are in phase equilibrium, and (6) reactions occur in the liquid phase. This method assesses the system's feasibility with the given phase equilibrium, reaction equilibrium, reaction extent, reflux ratio, and graphical information.

Figure 1(a) shows the composition profiles on a ternary diagram, which are graphical representations used to analyze the feasibility of an RD column with a rectifying reaction zone (nonisomolar combination reaction, $L + I \leftrightarrow H$), and Figure 1(b) presents a flowchart that systematizes the feasibility evaluation procedure. The numbers in parentheses within Figure 1(a,b) indicate the corresponding steps. First, the desired purities of the top (x_D) and bottom (x_B) products are determined, and then, the number of nonreactive (i) and reactive (j) stages are selected. Tray-by-tray calculations are performed with the distillate composition (x_D) when the reaction zone is located in the rectifying section. Figure 2

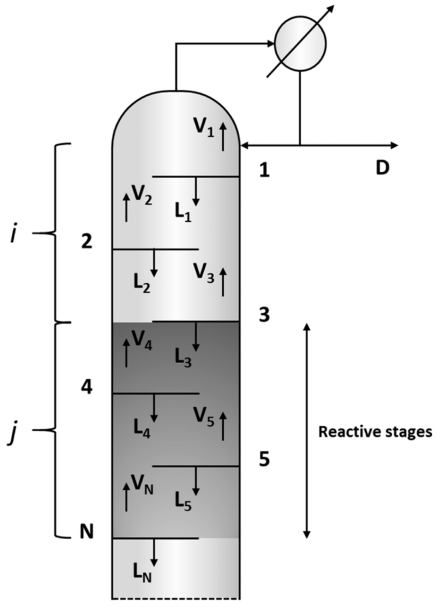

Figure 2. Schematic diagram of a rectifying section in a reactive distillation column.

shows a schematic diagram presenting the nonreactive stages (stage 1 to 3, $i = 3$) and reactive stages (stage 4 to N, $j = N - 3$), and the stage calculations are explained concerning this diagram. When a total condenser is used, x_D represents the composition of the vapor at the first stage (y_1); therefore, the vapor composition (y_1) is identical to x_D. Because the liquid flow at the first stage (L_1) is in phase equilibrium with the vapor flow (V_1), its liquid composition (x_1) can be calculated through a dew point calculation. The material balance at the first stage enables the vapor composition at the second stage (y_2) to be determined by using x_1 and x_D. This process is repeated for the number of nonreactive stages to perform the next-stage calculation of x_2, y_3, x_3, and y_4.

At the fourth stage, dew point calculation can obtain the liquid composition (x_4). This is a critical aspect for the feasibility evaluation of an RD column. Since the reaction was assumed to occur in the liquid phase, the liquid compositions in the reactive stages must facilitate the forward reaction. In other words, the liquid composition (x_4) on the ternary diagram should be located in the forward reaction region concerning the reaction equilibrium curve.[30] If the liquid composition is not located in the forward reaction region, then it can be considered an infeasible design due to the insufficient or negative reaction extent. The vapor composition (y_5) can be calculated by the material balance regarding the reaction difference point, a mathematical artifact representing the flow generated by the reaction. By iterating the process above for each reactive stage, it is possible to obtain x_5,⋯, y_N. Afterward, x_N is calculated by a dew point calculation, and it can be assessed whether it is possible to achieve the desired purity at the bottom (x_B) through simple distillation. This evaluation can be performed by determining whether x_N is included in the

https://doi.org/10.1021/acsomega.3c08128
ACS Omega 2023, 8, 48413−48431

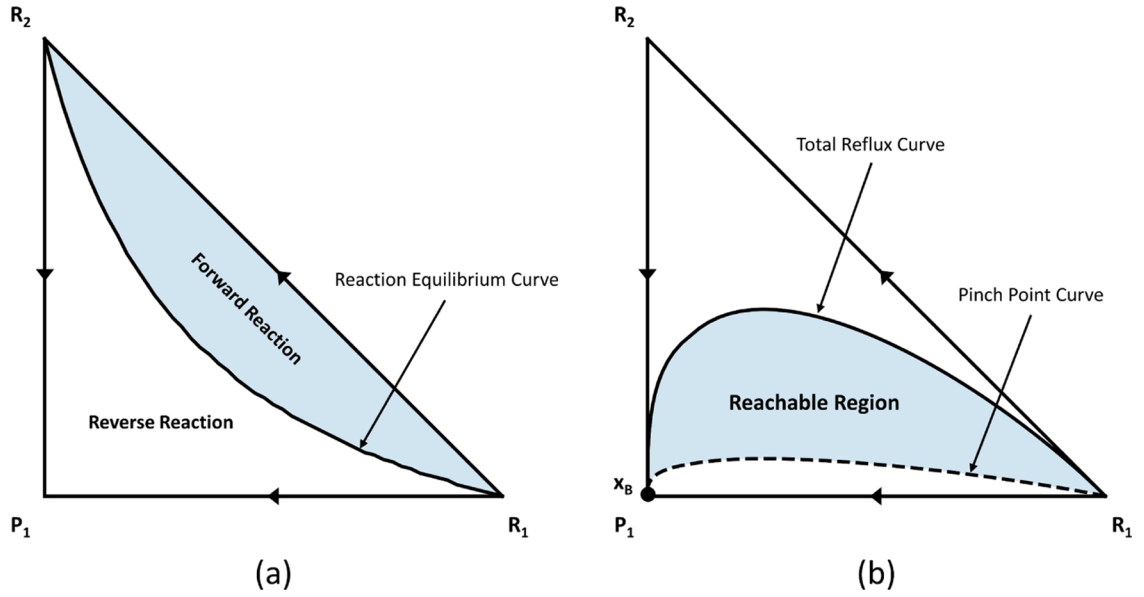

Figure 3. Ternary diagrams as the input images of segmentation for (a) the reaction region and (b) the reachable region. R_1: reactant 1, R_2: reactant 2, and P_1: product 1 ($R_1 + R_2 \leftrightarrow P_1$).

reachable region constructed through the total reflux curve and the pinch point curve based on the bottom product.[32] The RD column is considered feasible if x_N is located within the reachable region; otherwise, it is considered infeasible.

When there is a reaction zone in the stripping section, the feasibility evaluation can be performed in the opposite process to the rectifying section, using x_B as the initial composition. A detailed calculation process (phase equilibrium and material balance) and feasibility evaluation for the reaction zone located in the stripping section are covered in Section 3.

2.2. Geometry Recognition of a Ternary Diagram. The feasibility evaluation method involves interpreting the graphical information on a ternary diagram, which can be divided into three essential elements: (1) whether the liquid compositions at nonreactive stages move toward the forward reaction region, (2) whether the liquid compositions at reactive stages trigger a forward reaction, and (3) whether the liquid or vapor flow, after passing through the reaction zone, achieves the desired purity through simple distillation. Since the three elements mentioned above rely on the positional information of the compositions on the ternary diagram, the graphical information can be automatically interpreted if computers can recognize the ternary diagram. The current study proposed a novel method to recognize and evaluate the ternary diagram image using *k*-means clustering-based image segmentation,[46] which is a computer vision technique enabling the extraction and analysis of relevant graphical information, and the Canny edge detection algorithm.[47] The proposed method determines the followings: (1) whether the liquid composition at the reactive stage is located in the forward reaction region and (2) whether the liquid or vapor composition after the reaction zone falls within the reachable region.

2.2.1. Image Segmentation with K-Means Clustering. Image segmentation refers to partitioning an image into regions with the condition that each region should show homogeneity within itself. Furthermore, it is important that none of the border pixels are simultaneously occupied by two regions.[48] We distinguished regions on a pixel-by-pixel basis by utilizing the primary colors red (R), green (G), and blue (B). Figure 3 presents the input images for segmentation, in which the target region (forward reaction region in (a) and reachable region in (b)) is depicted in light blue (R, G, B: [210, 227, 240]). The ternary diagram image was segmented by applying the *k*-means clustering method to the RGB values of the pixels within the RGB color space.

K-means clustering is an unsupervised machine learning approach that seeks clustering data by identifying the centroids, which minimizes the sum of distances (clustering error) from the centroids to their closest points.[49] The clustering error can be represented as follows:

$$E = \sum_{j=1}^{k} \sum_{i=1}^{n} \| x_i^{(j)} - c_j \|^2 \tag{1}$$

where E is the clustering error, k is the number of clusters, n is the number of data points, $x_i^{(j)}$ is the data point in the cluster j, and c_j is the centroid of the cluster j. The RGB of each pixel was grouped into three clusters: (1) target region, (2) line, and (3) remaining area. The pixel accuracy, which represents the performance of the image segmentation, is calculated as follows

$$\text{pixel accuracy} = \frac{1}{k} \sum_{j=1}^{k} \frac{\text{TP}^{(j)} + \text{TN}^{(j)}}{\text{FP}^{(j)} + \text{FN}^{(j)} + \text{TP}^{(j)} + \text{TN}^{(j)}} \tag{2}$$

where k is the number of clusters, j is the cluster, TP is the true positive, TN is the true negative, FP is the false positive, and FN is the false negative.

Using red and green instead of blue to illustrate the target region generates the equivalent results in terms of pixel accuracy, as the Euclidean distances from black (0, 0, 0) to red (255, 0, 0), green (0, 255, 0), and blue (0, 0, 255) are equal. However, the pixel accuracy of segmentation is dependent on the brightness. The reason is that the performance is significantly influenced by the boundaries of the target region, which are determined by black lines. Pixel accuracy is determined at the intersection of the regions, where the

https://doi.org/10.1021/acsomega.3c08128
ACS Omega 2023, 8, 48413−48431

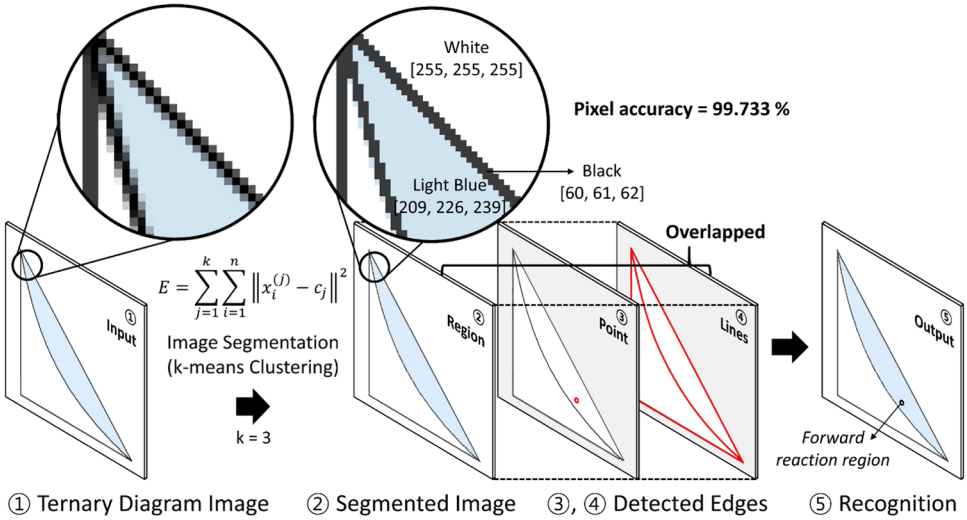

Figure 4. Procedure for proposed region recognition using *k*-means clustering-based image segmentation and the Canny edge detection algorithm.

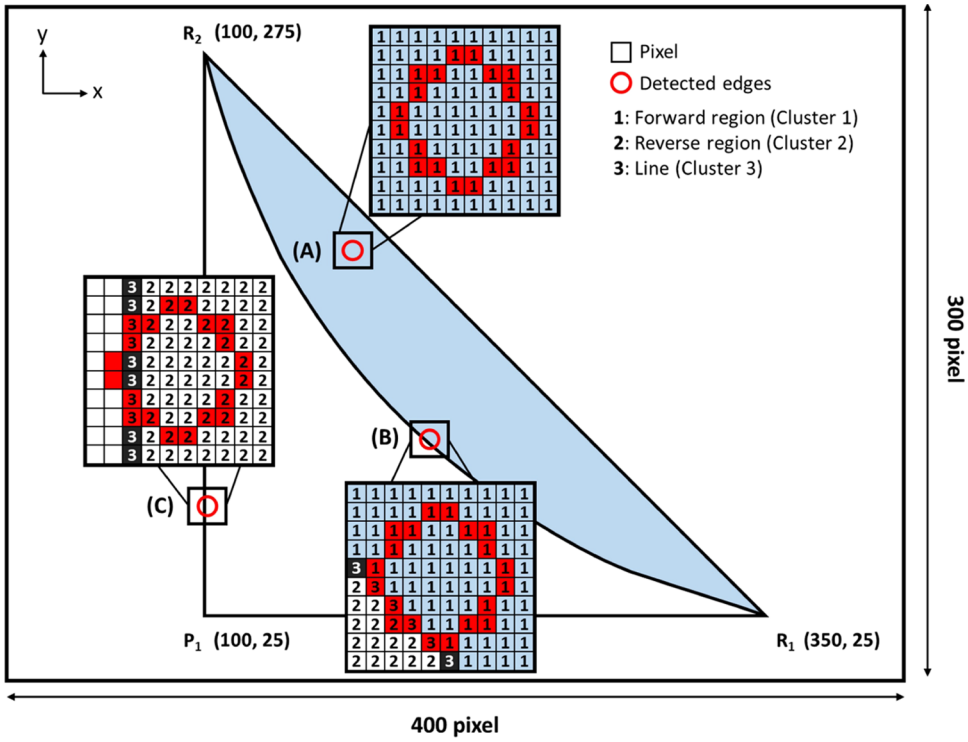

Figure 5. Examples of reaction region recognition results overlapping the segmented image with the detected edges.

boundaries gradually become brighter from black, causing the boundaries to become ambiguous and leading to difficulties in clustering. Since the number of pixels representing boundaries (lines) remains constant, the color variation of the boundary becomes more pronounced for colors far from black in the Euclidean distance. As a result, the spacing between points increases in the RGB space, leading to an improved clustering performance.

2.2.2. Canny Edge Detection. The Canny edge detection algorithm was applied to determine the locations of compositions that are required to be recognized in a ternary diagram image. A detailed explanation of the Canny edge detection algorithm is provided in the Supporting Information (Section S1). Furthermore, the algorithm was used to recognize the boundaries of the ternary diagram in the image, which were further used as a constraint condition. The detailed implementation of Canny edge detection in the region recognition of ternary diagram images for feasibility evaluation is explained in the following section.

2.2.3. Region Recognition. Region recognition begins with a ternary diagram image as input for image segmentation. The *k*-means clustering-based image segmentation algorithm is used to cluster pixels in each region. Figure 4 shows the reaction region recognition method through image segmentation and Canny edge detection. For *k*-means clustering, the parameters include the number of clusters (k), maximum iterations (maximum repetition limit), epsilon (the cluster radius), and the number of attempts (number of times the algorithm is executed with different labels). We tuned these parameters (max iterations, epsilon, and the attempts) through

https://doi.org/10.1021/acsomega.3c08128
ACS Omega 2023, 8, 48413−48431

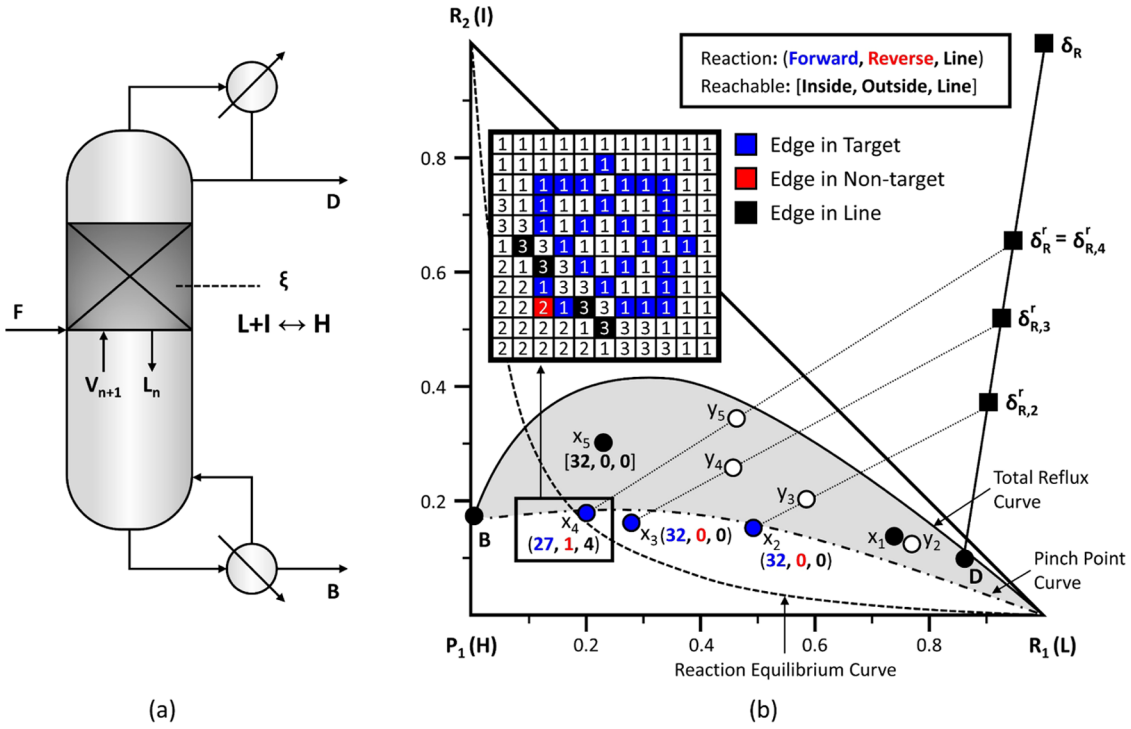

Figure 6. Feasibility evaluation of an RD column including 3 rectifying reactive stages: (a) schematic diagram of the RD column and (b) visualization of the feasibility evaluation result (feasible) with the recognized edge pixels. Blue circle: liquid composition in the forward reaction region, and shaded area: reachable region from the bottom product.

trial and error until achieving a pixel accuracy of 99%. Since the image is composed of the target region, nontarget region, and lines, the value of k in k-means clustering was set to three to categorize pixels into three clusters. In the segmented image, clusters were formed based on the three centroid colors (light blue: [209, 226, 239], white: [255, 255, 255], and black: [60, 61, 62]), and each pixel is filled with its centroid color, which makes the lines more prominent in terms of pixel appearance compared to the input image. The segmentation performance was represented by a pixel accuracy of 99.733%. Then, the point indicating the liquid composition at the reactive stage and the lines in the image are detected by the Canny edge detection algorithm to extract the positions of the edges. The recognized edges can be overlaid onto the segmented image to determine the region to which the edge pixels belong, and the cluster where the edge pixels are dominant is regarded as the region to which the liquid composition is affiliated. Figure 5 shows an example of reaction region recognition results using virtual liquid compositions (A, B, and C). The image (400 × 300 pixel) containing the ternary diagram (250 × 250 pixel) was segmented, and the detected edges of composition A, B, and C by the Canny edge detection algorithm were overlaid to classify each edge pixel.

In point (A), all of the edge pixels (marked in red) of the recognized liquid composition belong to the forward reaction region (cluster 1), indicating that a forward reaction occurs. In point (B), although the liquid composition slightly covers the reaction equilibrium curve, 15 edge pixels belong to the forward reaction region, 1 edge pixel belongs to the reverse region (cluster 2), and 4 edge pixels are on the line (cluster 3). Therefore, it also belongs to the forward reaction region where the largest number of pixels are located. In contrast, for composition (C), 14 pixels are located in the reverse reaction region and 4 pixels are on the line; thus, the result indicates that composition (C) lies on the reverse reaction region. Here, the detected edges enable us to recognize the ternary diagram boundaries in the image. The Canny edge detection algorithm was applied, resulting in the identification of the ternary diagram boundaries as lines: R_1 to R_2 (axis-x: 350 to 100, axis-y: 25 to 275), R_1 to P_1 (axis-x: 350 to 100, axis-y: 25), and P_1 to R_2 (axis-x: 100, axis-y: 25 to 275). The outer borderline provides a constraint, and pixels outside the lines are ignored. By the rule, the 2 pixels of composition (C) located outside the ternary diagram are disregarded. Thus, when the edges of the composition extend beyond a ternary diagram image, the total number of counted edge pixels decreases.

By employing image segmentation and edge detection techniques, automated recognition of the reaction region can be achieved. Similarly, the proposed methodology can be utilized for reachable region recognition. The application of the proposed region recognition method with stage calculations in the feasibility evaluation procedure, described in Section 3, enables the automated evaluation of an RD column based on the type of reaction.

3. RESULTS AND DISCUSSION

3.1. Ideal Mixtures with a Finite Reaction Difference Point. An ideal ternary mixture without azeotropes was assumed. Our approaches were described including the proposed region recognition method for evaluating the feasibility of a single-feed RD column with a nonisomolar combination reaction ($L + I \leftrightarrow H$). Here, the terms L, I, and H denote the light-, intermediate-, and heavy-boiling components, and the relative volatilities with respect to the heavy-boiling component were assumed to be 5, 3, and 1, respectively. Additional information is required to evaluate the feasibility of an RD column, such as a reaction equilibrium curve, total reflux curve, and pinch point curve. The reaction

https://doi.org/10.1021/acsomega.3c08128
ACS Omega 2023, 8, 48413−48431

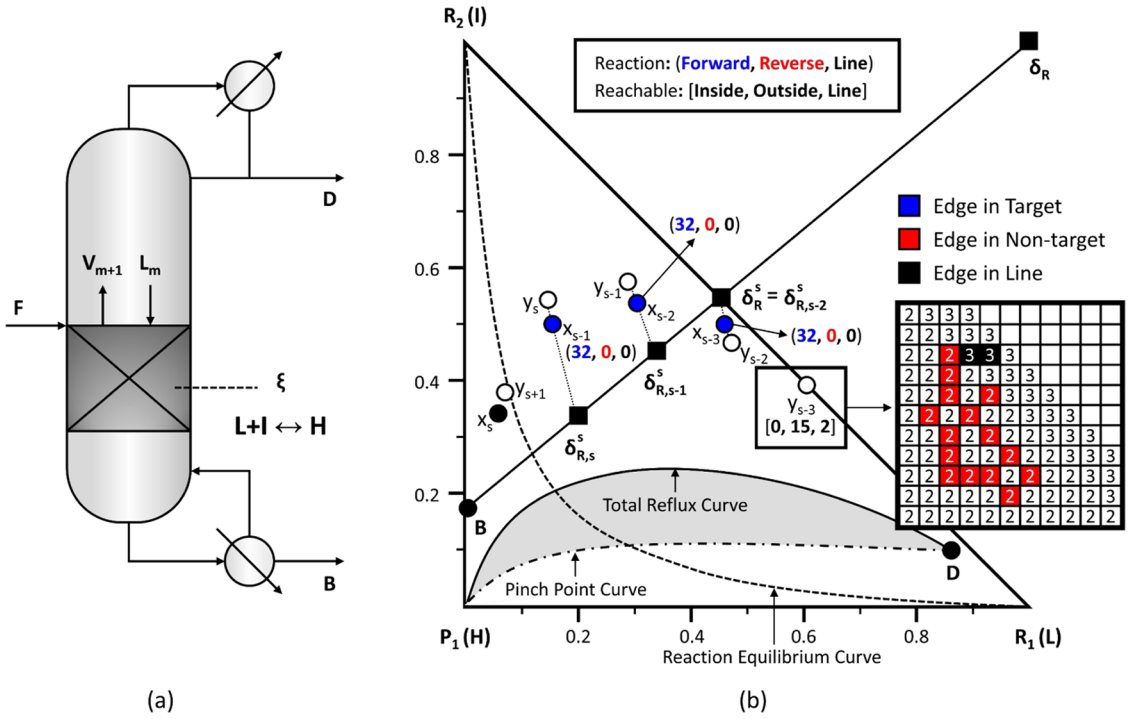

Figure 7. Feasibility evaluation of an RD column that has 3 stripping reactive stages: (a) schematic diagram of the RD column and (b) visualization of the feasibility evaluation result (infeasible) with the recognized edge pixels. Blue circle: liquid composition in the forward reaction region and shaded area: reachable region from the distillate product.

equilibrium curve indicates the concentrations at which all of the liquids are at both their boiling point and in a state of chemical equilibrium, which can be computed using the bubble point and chemical equilibrium calculation.[30] The residue curve can be used to estimate the total reflux curve for practical purposes because its difference is generally negligible with the distillation lines under total reflux in packed columns.[50] Finally, the pinch point curves are defined as mathematically colinear based on mass balances and phase equilibrium.[51] For phase equilibrium calculations, constant relative volatilities were assumed and the following equation was used:

$$y_{n,i} = \frac{\alpha_i x_{n,i}}{\sum_j \alpha_j x_{n,j}},\ i, j = L, I, H \tag{3}$$

where $y_{n,i}$ is the vapor composition of component i at stage n, $x_{n,i}$, and $x_{n,j}$ are the liquid compositions of components i and j at stage n, respectively, and α_i is the relative volatility of component i.

3.1.1. Feasibility Evaluation with a Rectifying Reaction Zone. For the feasibility evaluation, the reaction difference point (δ_R) and the total cascade difference point (δ_R^r and δ_R^s) were introduced by the material balances.[52] Material balances and reactive lever rules for an RD column with a rectifying reaction zone are provided in the Supporting Information (Section S2.1). As the stoichiometric coefficients vector of the given reaction is $[-1, -1, 1]$ (= $[L, I, H]$), the reaction difference point is calculated to be $[1, 1, -1]$, which is equal to $[-1, -1, 1]/(-1-1+1)$ by the definition of the reaction difference point. To ensure the feasibility of the RD column, all liquid compositions at a reaction zone should locate within the forward reaction region, and the liquid composition that passes through the reaction zone should be within the reachable region. Additionally, the reactive cascade difference point ($\delta_{R,n}^r$) of the reactive rectifying section, which represents the accumulated reaction turnover, should move toward the total cascade difference point (δ_R^r).

Figure 6(a) shows a schematic diagram of an RD column with a rectifying reaction zone. The feasibility evaluation involves tray-by-tray calculations based on the phase equilibrium and material balance starting from the distillate composition (x_D). Figure 6(b) shows the feasibility evaluation result of the RD column with one rectifying stage and three reactive stages. The proposed evaluation method utilizes the reaction equilibrium curve (K_{eq} = 20), reachable region, reaction difference point, total reactive difference point, reactive cascade difference point, and desired product compositions.

First, ternary diagram image segmentation and Canny edge detection were performed. The segmentation results calculated by eq 2 showed an accuracy of 99.737% for the reaction region and 99.879% for the reachable region. Afterward, the stage calculation was initiated by the desired distillate composition. The phase equilibrium calculation by eq 3 was carried out for a given distillate composition to obtain the liquid composition (x_1), and the vapor composition (y_2) was determined using the lever rule (L_1/D) between the liquid composition (x_1) and distillate composition (x_D). Similarly, the liquid composition (x_2) was calculated through the phase equilibrium calculation, and whether the liquid composition is in the forward reaction region. Through the region recognition, 32 edge pixels were found on the right side of the reaction equilibrium curve (indicating the forward reaction). In comparison, 0 pixels were detected on the left side (indicating the reverse reaction) and line, denoted as (32, 0, 0). The identification of the reaction region indicated that the liquid composition (x_2) exists within the forward reaction region implying that the forward reaction occurs at the second stage. Since the liquid composition (x_2) is within the forward reaction zone, the vapor composition (y_3) is

https://doi.org/10.1021/acsomega.3c08128
ACS Omega 2023, 8, 48413−48431

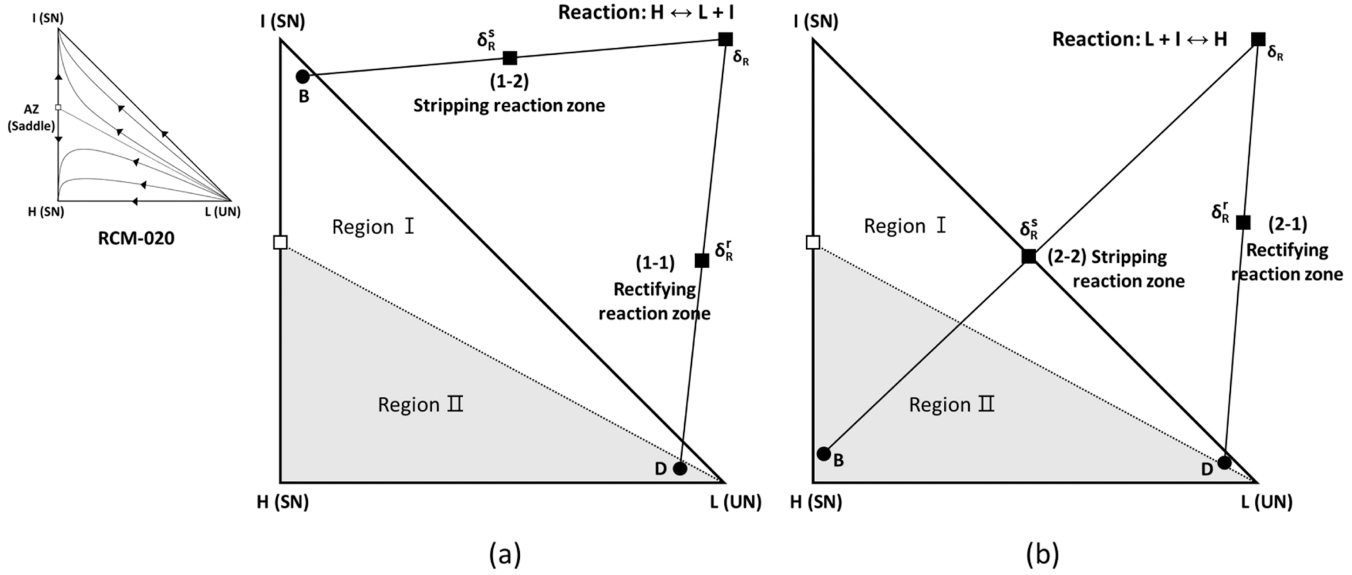

Figure 8. Descriptions of the ternary system and physical properties, including a minimum-boiling azeotrope (RCM-020): (a) cases with a decomposition reaction, $H \leftrightarrow L + I$ and (b) cases with a combination reaction, $L + I \leftrightarrow H$.

determined by the reactive lever rule ($L_2/D - \nu_T\xi_2$), as it lies on a straight line connecting the reactive cascade difference point ($\delta_{R,2}{}^r$) and the liquid composition at stage 2 (x_2). The same procedure was repeated to calculate the liquid and vapor compositions (x_3, y_4, x_4, y_5, x_5), revealing that all of the liquid compositions in the reactive stages, x_3: (32, 0, 0) and x_4: (27, 1, 4), are located in the forward reaction region. In addition, all edge pixels of the liquid composition (x_5) that passed through the reaction zone are located within the reachable region, x_5: [32, 0, 0], indicating that the RD column is a feasible design that satisfies the desired bottom purity. The feasibility evaluation of the RD column with the ternary diagram can be performed automatically with the region recognition, and the computational time required for the feasibility evaluation was 1.53 s.

3.1.2. Feasibility Evaluation with a Stripping Reaction Zone. Figure 7(a) illustrates a schematic diagram of an RD column with a stripping reaction zone; the material balance and reactive lever rules for the RD column are provided in the Supporting Information (Section S2.2). Figure 7(b) describes the feasibility evaluation of the RD column with one stripping stage and three reactive stages, and all other conditions are equivalent to those in the rectifying case that was previously discussed. As a result of the segmentation, it was determined that the reaction region coincides with the rectifying case (K_{eq} = 20), and the reachable region was found to have a pixel accuracy of 99.729%. The feasibility evaluation of the RD column was performed by bottom-up stage calculations from the desired bottom composition (x_B) in contrast to that of the rectifying case.

In the reboiler, because the vapor in equilibrium with the bottom product is supplied to the column, the vapor composition (y_{s+1}) can be computed by using the phase equilibrium (eq 3) with the bottom composition. The liquid composition (x_s) at stage s is located between the bottom composition (x_B) and the vapor composition (y_{s+1}) according to the lever rule (V_{s+1}/B). With phase equilibrium, the vapor composition (y_s) can be computed. The liquid composition (x_{s-1}) at a reactive stage lies on the line between the reactive cascade difference point ($\delta_{R,s}{}^s$) and the vapor composition (y_s) by the reactive lever rule ($V_s/B - \nu_T\xi_s$). The liquid composition (x_{s-1}) is located in the forward reaction region, with 32 pixels in the forward region and 0 pixels on the reverse reaction region and line, respectively, denoted as (32, 0, 0). The remaining liquid and vapor compositions (y_{s-1}, x_{s-2}, y_{s-2}, x_{s-3}, y_{s-3}) can be found, and all liquid compositions are placed within the forward reaction region, x_{s-2}: (32, 0, 0) and x_{s-3}: (32, 0, 0). However, the edges of the vapor composition (y_{s-3}) that have passed through the reaction zone belong to 0 pixels inside, 15 pixels outside the reachable region, and 2 pixels on the line, [0, 15, 2], which indicates that the RD column is infeasible under the given conditions. The feasibility evaluation of the RD column by the proposed method had a computation time of 1.51 s.

3.2. Azeotropic Mixtures with a Finite Reaction Difference Point. A detailed feasibility evaluation was carried out for azeotropic ternary mixtures with distillation boundaries. The RCM-020 system was used as an example for the feasibility evaluation in this section. The RCM-020 system has a minimum-boiling azeotrope between the light and heavy components, and there are two distillation regions.[53] As singular points were classified according to the characteristics of the RCM in terms of stability, the azeotrope was identified as a saddle, the light component as an unstable node (UN), and both the heavy component and intermediate component as stable nodes (SN).[54] According to the RD feasibility criteria, if products are UN and SN, respectively, and they are in the same distillation region, an RD column is feasible regardless of the location of the reaction zone in either the rectifying or stripping section.[32]

Here, the feasibility was evaluated when the products were in different distillation regions under the same system. To compute the phase equilibrium, a specific mixture was chosen to calculate the physical properties and phase equilibrium by using Aspen Plus V11. The binary parameters of the mixture are described in the Supporting Information (Section S4.1). The feasibility evaluation was conducted for the two cases based on nonisomolar reaction forms: the decomposition reaction ($H \leftrightarrow L + I$) and the combination reaction ($L + I \leftrightarrow H$). It was assumed that the reaction occurs in two reactive

https://doi.org/10.1021/acsomega.3c08128
ACS Omega 2023, 8, 48413−48431

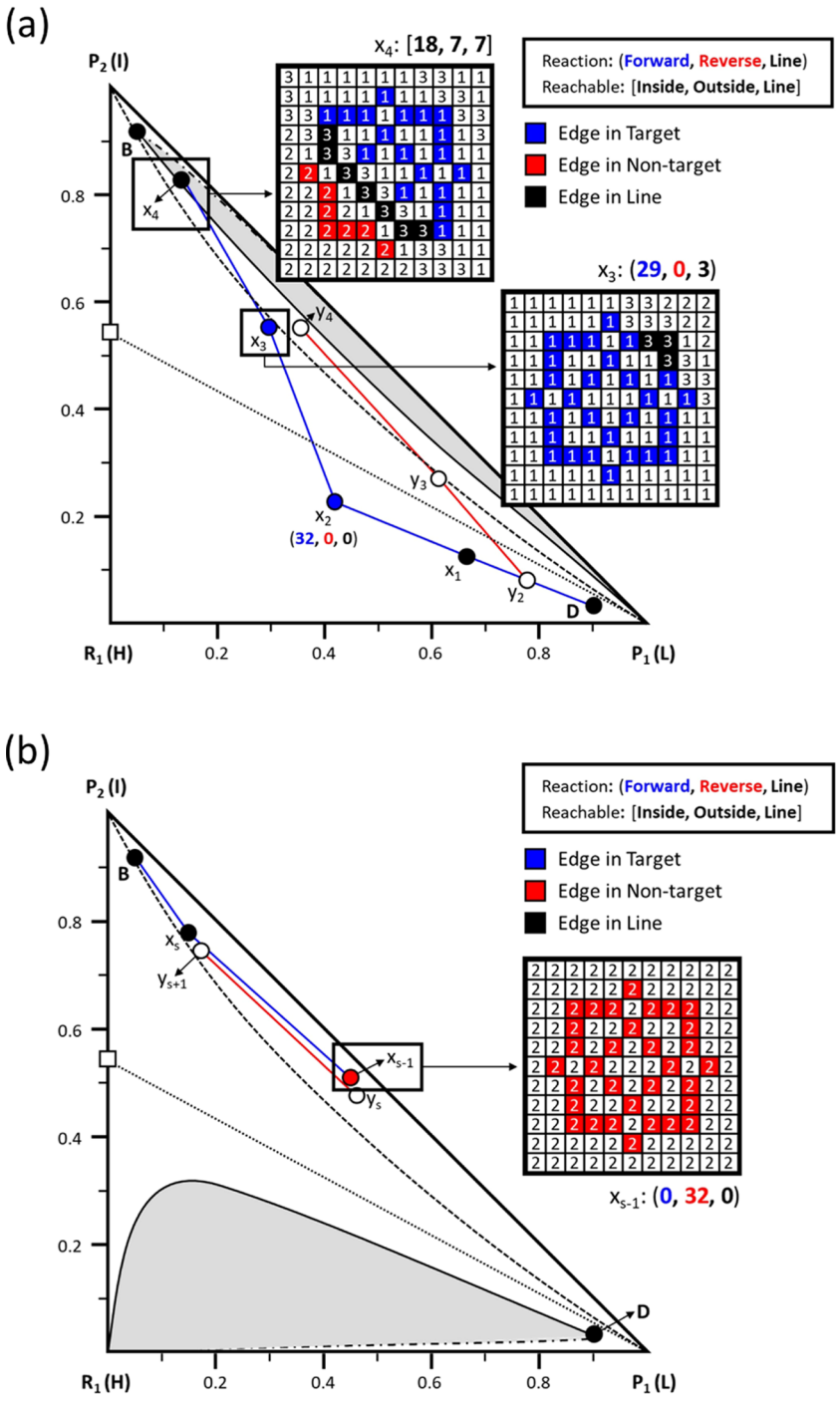

Figure 9. Region recognition and feasibility evaluation results of the RD column with the nonisomolar decomposition reaction ($H \leftrightarrow L + I$) in the (a) rectifying section-feasible and (b) stripping section-infeasible for the RCM-020 ternary system. Blue circle: liquid composition in the forward reaction region, red circle: liquid composition in the reverse reaction region, and shaded area: reachable region from the desired top or bottom product.

stages, and the molar turnover (90% conversion) in each stage is the same as in all cases.

Figure 8(a) shows a scenario in which a decomposition reaction occurs, and the desired products are located in different distillation regions (x_D: region II, and x_B: region I). The feasibility evaluation was conducted to confirm the possibility of circumventing the distillation boundary for cases where the reaction zone is located in the rectifying section (case 1−1) and in the stripping section (case 1−2), respectively. Since the products in case 1−1 lie in different distillation regions; thus, it is necessary to circumvent the distillation boundary to achieve the desired purity. The reaction difference point is defined as $[1, 1, -1]$ by stoichiometric coefficients, and the total/reactive cascade difference points are located on the line connecting the distillate composition and the reaction difference point. The segmentation and feasibility evaluation results of case 1−1 are shown in Figure 9(a). The stage calculations started from the distillate composition, and the possibility of a forward reaction occurring at the reactive stage was confirmed using the

https://doi.org/10.1021/acsomega.3c08128
ACS Omega 2023, 8, 48413−48431

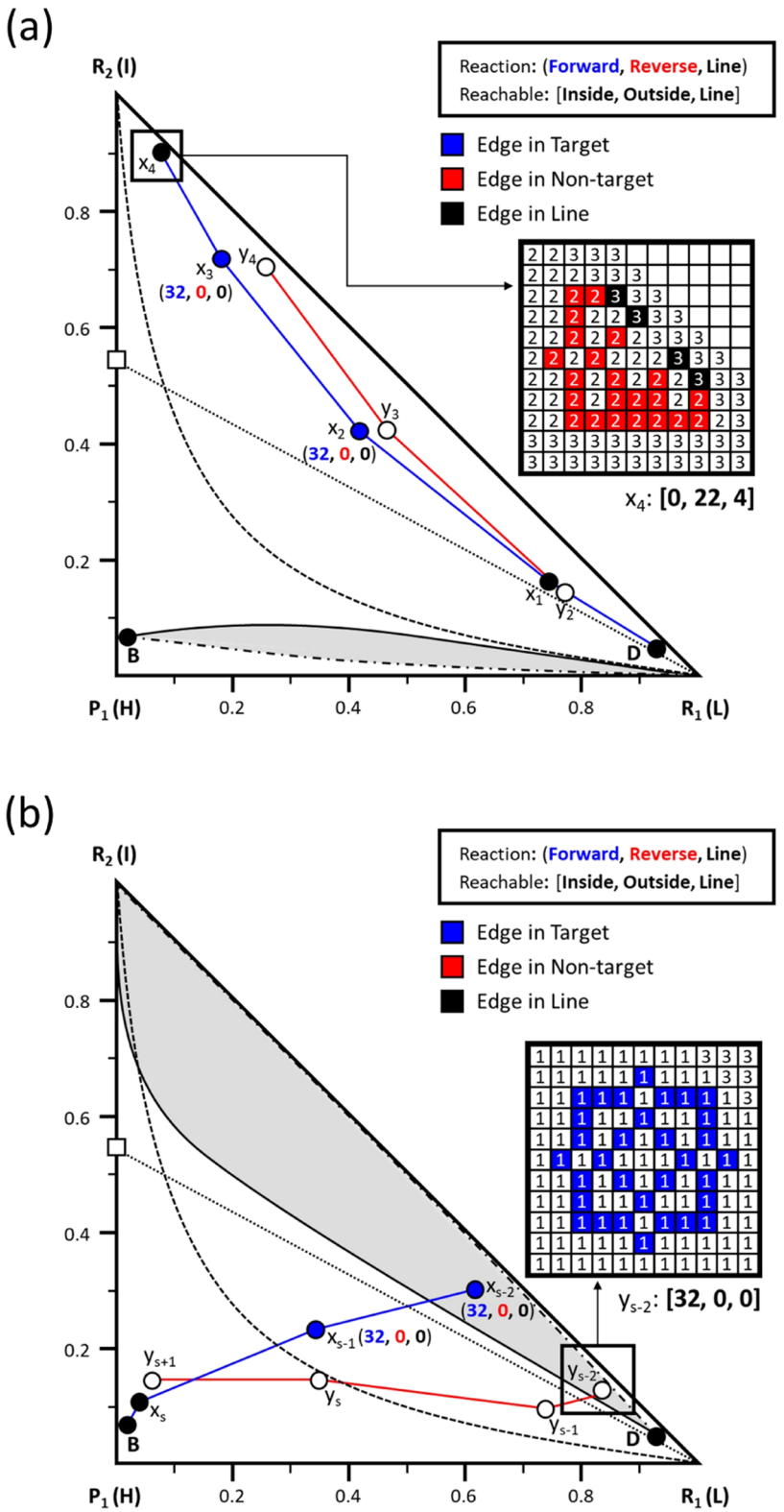

Figure 10. Region recognition and feasibility evaluation results of the RD column with the nonisomolar combination reaction ($L + I \leftrightarrow H$) in the (a) rectifying section-infeasible, and (b) stripping section-feasible for the RCM-020 ternary system. Blue circle: liquid composition in the forward reaction region, red circle: liquid composition in the reverse reaction region, and shaded area: reachable region from the desired top or bottom product.

proposed region recognition method. The segmentation result for the reaction region showed an accuracy of 99.726%, and both liquid compositions (x_2, x_3) were located in the forward reaction region as x_2: (32, 0, 0) and x_3: (29, 0, 3). The forward reaction occurs at all reactive stages, and the vapor compositions are located on the straight line connecting the liquid composition and the reactive cascade difference point, as determined by the reactive lever rule. According to the result,

https://doi.org/10.1021/acsomega.3c08128
ACS Omega 2023, 8, 48413−48431

Table 1. Parameters and Results of the RD Feasibility Evaluation with Nonisomolar Reactions for the RCM-020 System

parameters	case 1−1	case 1−2	case 2−1	case 2−2
reaction zone	rectifying	stripping	rectifying	stripping
reactive stages no.	2	2	2	2
reaction type	decomposition	decomposition	combination	combination
equilibrium constant	1.5	1.5	10	10
reflux/boil-up ratio	1.3	20	20	3
feed composition	[0.00, 0.00, 1.00]	[0.00, 0.00, 1.00]	[0.60, 0.40, 0.00]	[0.60, 0.40, 0.00]
distillate composition	[0.90, 0.03, 0.07]	[0.90, 0.03, 0.07]	[0.92, 0.04, 0.04]	[0.92, 0.04, 0.04]
bottom composition	[0.05, 0.92, 0.03]	[0.05, 0.92, 0.03]	[0.01, 0.07, 0.92]	[0.01, 0.07, 0.92]
feed rate (kmol/h)	5	5	10	10
distillate rate (kmol/h)	4.75	4.75	2.6	2.6
bottom rate (kmol/h)	4.75	4.75	3.8	3.8
reaction extent (kmol)	4.5	4.5	3.6	3.6
pixel accuracy (%) [reaction, reachable]	99.726, 99.837	99.726, 99.645	99.719, 99.323	99.719, 99.812
feasibility	feasible	infeasible	infeasible	feasible
computation time (s)	3.16	2.85	3.01	3.03

the composition can move from region II to region I, and as the stage moves down the column, the composition moves toward the stable node which is the intermediate component (P_2). Finally, the liquid composition (x_4) that passes through the reaction zone must be located within the reachable region. To evaluate the reachability to the desired bottom product, the segmentation of the reachable region was performed, which showed an accuracy of 99.837%, and the recognition result was [18, 7, 7], indicating that the liquid composition (x_4) is located within the reachable region. Therefore, the RD column is a feasible design that can produce the desired top and bottom products by crossing the distillation boundary. The result was obtained in 3.16 s using the proposed automated method.

On the other hand, Figure 9(b) presents the results of case 1−2, which includes a stripping reaction zone. The total/reactive cascade difference points are located on the line connecting the bottom composition and the reaction difference point, and the stage calculations were performed starting from the bottom composition. In this case, the liquid composition (x_{s-1}) is located in the reverse reaction region (0, 32, 0). The composition profile cannot cross the distillation boundary and moves toward the unstable node of region I as the stage moves up the column. Thus, the RD column is an infeasible design, and the evaluation took 2.85 s.

Figure 8(b) shows cases that include RD columns with a combination reaction ($L + I \leftrightarrow H$), which has the reaction difference point defined as [1, 1, −1], and the desired products are located in different distillation regions (x_D: region I, and x_B: region II). Figure 10(a) shows an RD column in which a combination reaction is taking place in a rectifying reaction zone (case 2−1). When the stage calculations were performed from the distillate composition, all liquid compositions (x_2, x_3) of the reactive stages are located in the forward reaction region as (32, 0, 0). However, the composition profile approaches the intermediate-boiling component, which is a stable node in region I, as the stage moves downward of the RD column because the composition profile cannot cross the distillation boundary. The liquid composition (x_4) is not located within the reachable region, as the recognition result is [0, 22, 4]. Therefore, the RD column under the given specification is an infeasible design.

Conversely, Figure 10(b) represents an RD column with a stripping reaction zone (case 2−2), and the tray-by-tray calculations were performed starting from the bottom composition. The liquid compositions (x_{s-1}, x_{s-2}) at all reactive stages are located in the forward reaction region, and the distillation boundary is crossed due to the forward reaction. After the reaction zone, the compositions move toward the desired distillation composition as the stage goes up the column, and the recognition result shows that the vapor composition (y_{s-2}) is located in the reachable region, [32, 0, 0]. Hence, this RD column is a feasible design, and the proposed method took 3.03 s to evaluate the feasibility. The detailed conditions and results of the feasibility evaluation are listed in Table 1.

In an RD column with the nonisomolar reaction, the vapor or liquid compositions can cross the distillation boundary depending on the direction from the product (D or B) to the reaction difference point, when it is assumed that the reaction has occurred sufficiently and the forward reaction region covers multiple distillation regions. The compositions in reactive stages are determined based on the reactive cascade difference point by the material balance, and the reactive cascade difference point is located on a straight line connecting the desired product and the reaction difference point, which means that the position of reactive cascade difference point depends on the location of the desired product and the reaction difference point. Consequently, graphical interpretation shows that if the distillation boundary or its extension line is positioned between the reaction difference point and the desired product (x_D or x_B), the compositions can cross the boundary. The proposed automated feasibility evaluation algorithm enables the assessment of the feasibility of RD columns within seconds, using only specific parameters without the need for graphical interpretation.

3.3. Azeotropic Mixtures with an Infinite Reaction Difference Point. The reaction difference point is a mathematical artifact that enables the interpretation of composition changes by reactions on RCMs. However, since the reaction difference point represents the molar flow rate changes, an isomolar metathesis reaction ($2I \leftrightarrow L + H$), which has no difference in the number of moles between reactants and products, leads to an infinite reaction difference point: [1, −2, 1]/(1−2+1) = [∞, −∞, ∞]. Consequently, the reaction difference point cannot be represented in the composition space. To address this limitation, a series of transformations are required which involves dividing the chemical stoichiometric coefficients into reactant and product components.[52] The

https://doi.org/10.1021/acsomega.3c08128
ACS Omega 2023, 8, 48413−48431

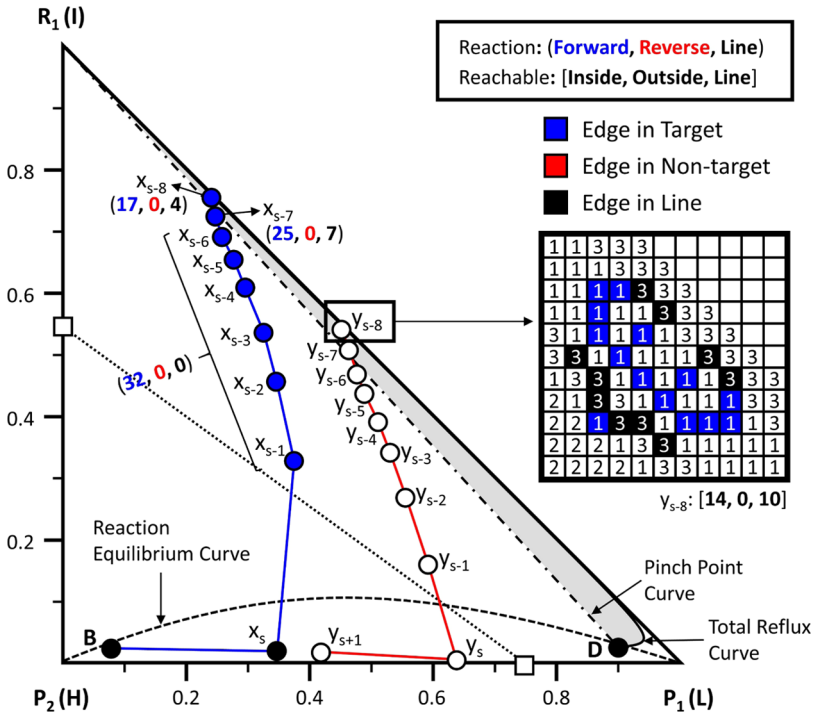

Figure 11. Feasible design of an RD column with the isomolar metathesis reaction ($2I \leftrightarrow L + H$) in the stripping section for the RCM-021 system.

material balance and reactive lever rules for an RD column including the infinite reaction difference point are provided in the Supporting Information (Section S3). And a specific mixture for the RCM-021 system was chosen to calculate the physical properties and phase equilibrium. The mixture for the Aspen Plus calculation is described in the Supporting Information (Section S4.2), and the feasibility evaluation results (case 3−1: rectifying reaction zone; case 3−2: stripping reaction zone) are explained based on the location of the reaction zone for the RCM-021 system in the Supporting Information (Section S5).

According to the feasibility criteria, if one of the products in the RD column with the isomolar decomposition reaction is a saddle and an azeotrope exists between products (e.g., RCM-021, RCM-210, RCM-430, and RCM-340), the RD column design is infeasible regardless of the reaction zone. However, in the RCM-021 system, if the vapor composition that passes through the reaction zone is located on the $L-I$ edge, then a pure light component can be produced through simple distillation. In the RD column with a stripping reaction zone, liquid and vapor compositions move toward the L and I edges due to the position of the reactive cascade difference points. Figure 11 shows a feasible design obtained through the feasibility evaluation. It has one stripping stage and eight reactive stages, assuming 98% conversion at the reaction zone (reaction extent at each reactive stage: 4.83, 4.84, 4.85, 4.86, 4.87, 4.88, 4.89, and 4.90 kmol). The liquid compositions are located in the forward reaction region at all stages, and the vapor composition (y_{s-8}), which is located close to the $L-I$ edge is on the reachable region, y_{s-8}: [14, 0, 10], which makes it a feasible design. We have rigorously validated the capability of the vapor composition (y_{s-8}) to achieve the desired distillate purity through an Aspen Plus simulation. The detailed results of the simulation are provided in the Supporting Information (Section S6). This case shows that the design is feasible when one of the products is a saddle, there is an azeotrope between the products, which requires sufficient reactive stages and conversion, and the molar turnover rate at the stage closest to the product stream must be greater than that of the feed stage. The parameters and results of the feasible example for the RCM-021 system with an infinite reaction difference point are shown in Table 2.

Table 2. Parameters and Results of the RD Feasibility Evaluation with Isomolar Reactions for the RCM-021 System (Feasible Example)

parameters	RCM-021 example
reaction zone	stripping
reactive stages no.	8
reaction type	metathesis
equilibrium constant	2
reflux/boil-up ratio	5
feed composition	[0.00, 1.00, 0.00]
distillate composition	[0.90, 0.02, 0.08]
bottom composition	[0.08, 0.02, 0.90]
feed rate (kmol/h)	10
distillate rate (kmol/h)	5
bottom rate (kmol/h)	5
reaction extent (kmol)	4.90
pixel accuracy (%) [reaction, reachable]	99.755, 99.881
feasibility	feasible
computation time (s)	6.14

It should be noted that since the RD feasibility criteria are necessary conditions, the criteria cannot guarantee the feasibility in all cases when one of the products is saddled with an azeotrope between the products. This limitation of the criteria highlights the need for a detailed feasibility evaluation of each system, considering specific characteristics of the RD system such as the reaction and phase equilibrium, reaction extents, and number of reactive stages.

https://doi.org/10.1021/acsomega.3c08128
ACS Omega 2023, 8, 48413−48431

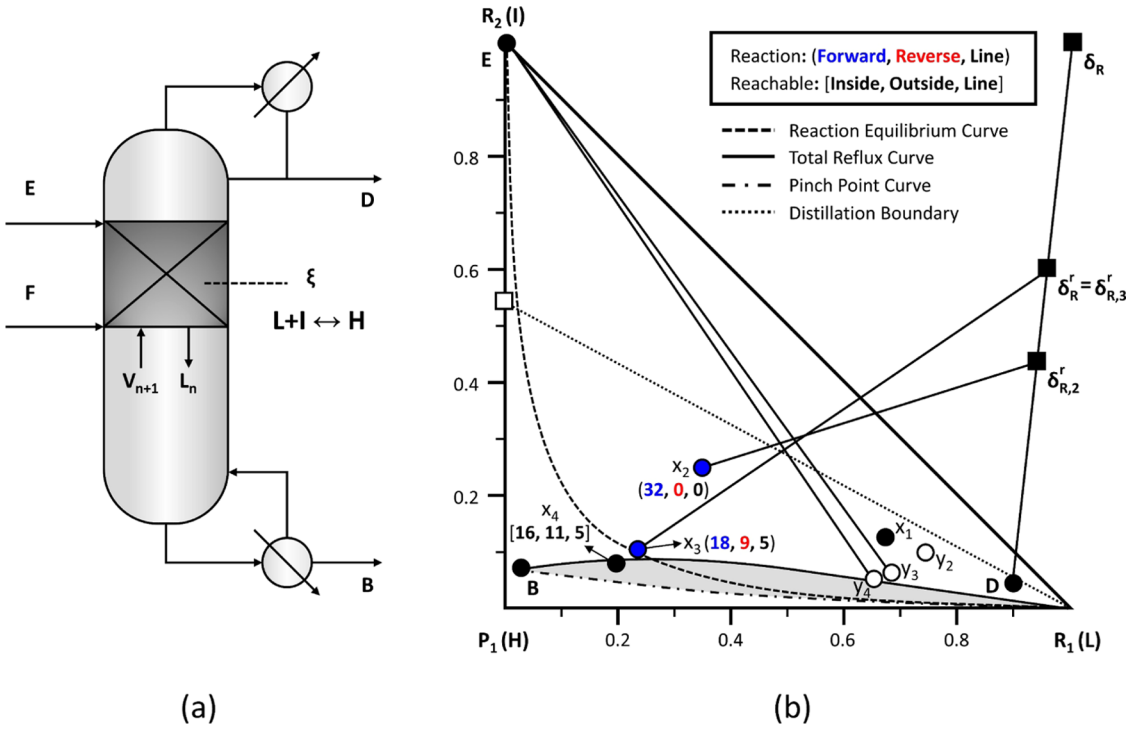

Figure 12. Feasibility evaluation of a double-feed RD column including 2 rectifying reactive stages: (a) schematic diagram of the RD column and (b) visualization of the feasibility evaluation result (feasible). Blue circle: liquid composition in the forward reaction region and shaded area: reachable region from the distillate product.

3.4. Double-Feed Reactive Distillation Column. Figure 12(a) indicates a schematic diagram of a double-feed RD column with a rectifying reaction zone. Its feasibility can also be assessed by using the proposed approach. The material balance and reactive lever rules for a double-feed RD column are provided in the Supporting Information (Section S2.3). The feasibility evaluation result of the double-feed RD column is presented in Figure 12(b). The evaluated design maintains a consistent assumption comprising a single nonreactive stage and two reactive stages, with equal molar turnover in each reactive stage. Given the presence of the reaction zone in the rectifying section, stage calculations were performed from the distillate composition. The computed liquid composition (x_2) of the initial reactive stage is situated within the forward reaction region, x_2: (32, 0, 0). Consequently, the lever rule, derived from eqs (S25) and (S26) in the Supporting Information, shows that the vapor composition (y_3) passes the intersection point on the straight line connecting the liquid composition (x_2) and the reactive cascade difference point, and extends along the straight line originating from the upper feed composition (x_E). Moreover, using a dew point calculation for the resulting vapor composition (y_3) determines the liquid composition (x_3) in the second reactive stage, which also lies within the forward reaction region, x_3: (18, 9, 5). The examined double-feed column satisfies the requirement for an adequate level of reaction. Furthermore, the liquid composition (x_4) is located within the reachable region, x_4: [16, 11, 5], which verifies the feasibility of the design. Notably, the feasibility evaluation including stage calculations of the RD column required approximately 3.01 s, implying the potential for conducting a timely feasibility evaluation for double-feed columns. Similarly, a reverse process can be applied when the reaction zone is located in a stripping section.

4. CASE STUDIES

4.1. Finite Reaction Difference Point: Methyl *tert*-Butyl Ether (MTBE) Synthesis. Methyl *tert*-butyl ether (MTBE) is produced in a nonisomolar combination reaction, where isobutene (IBUT) reacts with methanol (MeOH).[55] This reaction presents a finite reaction difference point on the ternary diagram. The first case study focused on an RD column designed for MTBE synthesis, comprising two rectifying stages and six reactive stages (3 to 8 stages).

Figure 13(a) shows the feasibility evaluation result of the RD column for the production of MTBE. The reactive stages 3 to 8 and liquid composition passing through the reaction zone are shown. The RD column operates with a reaction zone located in the rectifying section, employing stage calculations starting from distillate composition. The liquid compositions of the first to third reactive stages (x_3, x_4, x_5) are situated near the distillate composition and are placed within the forward reaction zone. Furthermore, liquid compositions (x_6, x_7, and x_8) in the remaining reactive stages, as shown in Figure 13(a), exist within the forward reaction region. It is noteworthy that the liquid composition (x_9) also falls within the reachable region, confirming the feasibility of the RD column design. The detailed pixel recognition results for the MTBE synthesis are listed in Figure 13(b). The result was further validated through rigorous simulation using Aspen Plus.

Figure 13(c) presents a comparative analysis of the liquid profiles between the simulation results and the calculated results. Detailed conditions (thermodynamic model, binary coefficients, reaction kinetics, and chemical equilibrium constant) for the rigorous simulation in Aspen Plus are provided in the Supporting Information (Section S7.1). Remarkably, the calculated results closely aligned with the simulation results obtained using Aspen Plus. Furthermore,

https://doi.org/10.1021/acsomega.3c08128
ACS Omega 2023, 8, 48413−48431

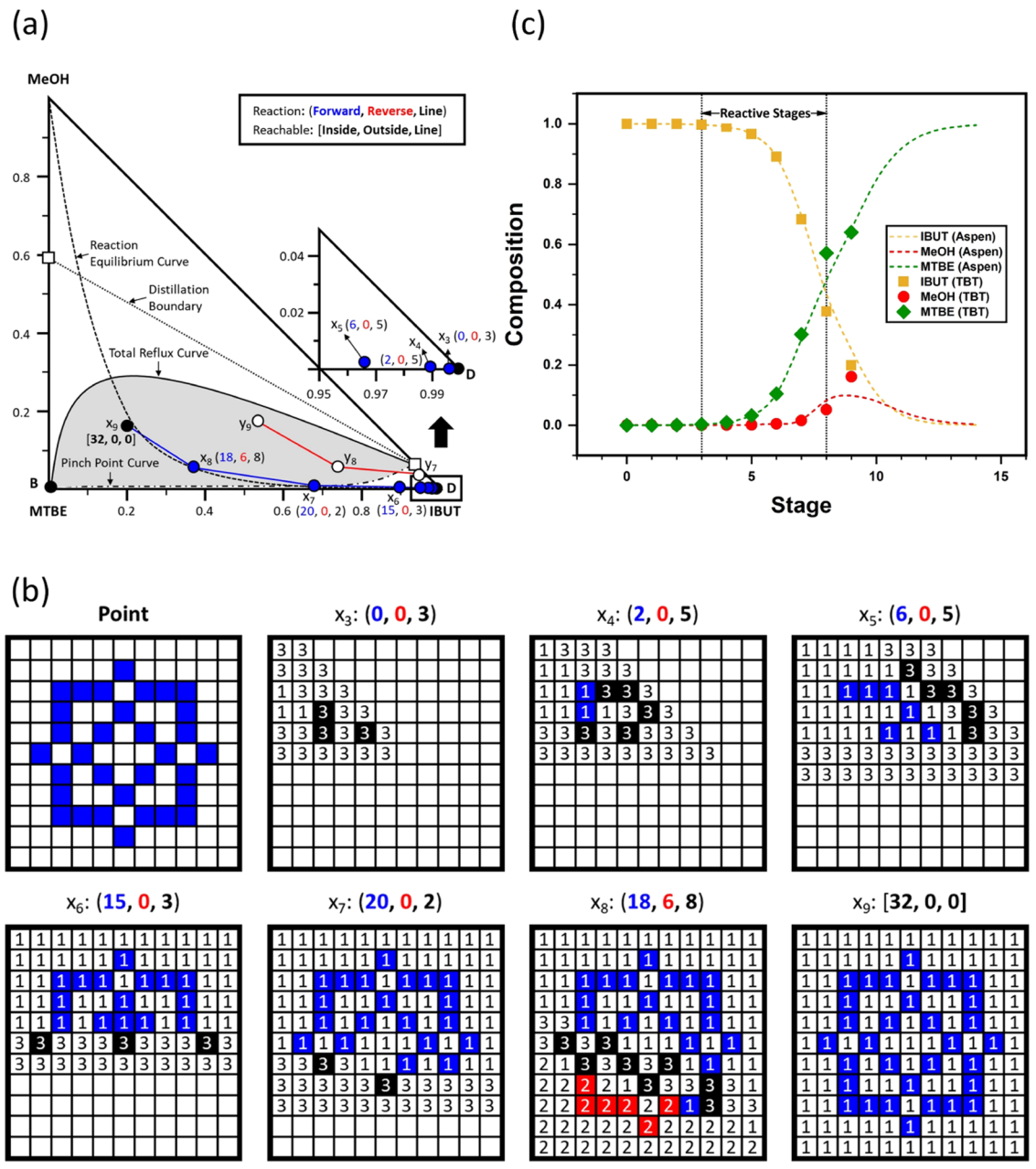

Figure 13. (a) Feasibility evaluation results of the RD column for the production of MTBE, (b) detailed results for the recognized edges of the liquid compositions of the MTBE synthesis RD column, and (c) comparison of the liquid composition profile between the rigorous simulation and tray-by-tray (TBT) calculations.

during the column simulation, a bottom product with an MTBE purity of over 99.5% was achieved, thereby providing confirmation of the design feasibility through rigorous simulation.

4.2. Infinite Reaction Difference Point: 2-Pentene Metathesis. The second case study involved the feasibility evaluation of an RD column for the metathesis reaction of 2-pentene. The reaction entails the metathesis of 2-pentene (2 mol) into 2-butene and 3-hexene, each with a stoichiometric ratio of 1 mol, representing an isomolar metathesis reaction.[56] Consequently, the system exhibits an infinite reaction difference point. The metathesis reaction of 2-pentene occurs in the stripping section, and the design feasibility of an RD column with four stripping stages and seven reactive stages was assessed.

Figure 14(a) shows the result of the feasibility evaluation for the RD column, highlighting the reactive stages (10 to 16 stage) and vapor composition (y_{10}), representing the graphical information. Starting from the bottom composition, tray-by-tray calculations progress upward with the liquid and vapor compositions in the stripping section following the reaction equilibrium curve, and the liquid compositions (x_{10} to x_{16}) in the reactive stages indicate a similar shape along the reaction equilibrium curve. Based on the results of the region recognition, it was observed that all liquid compositions of the reactive stages reside within the forward reaction region and the vapor compositions (y_{10}) also fall within the reachable region. The detailed pixel recognition results for the 2-pentene metathesis are shown in Figure 14(b). Therefore, it can be

https://doi.org/10.1021/acsomega.3c08128
ACS Omega 2023, 8, 48413−48431

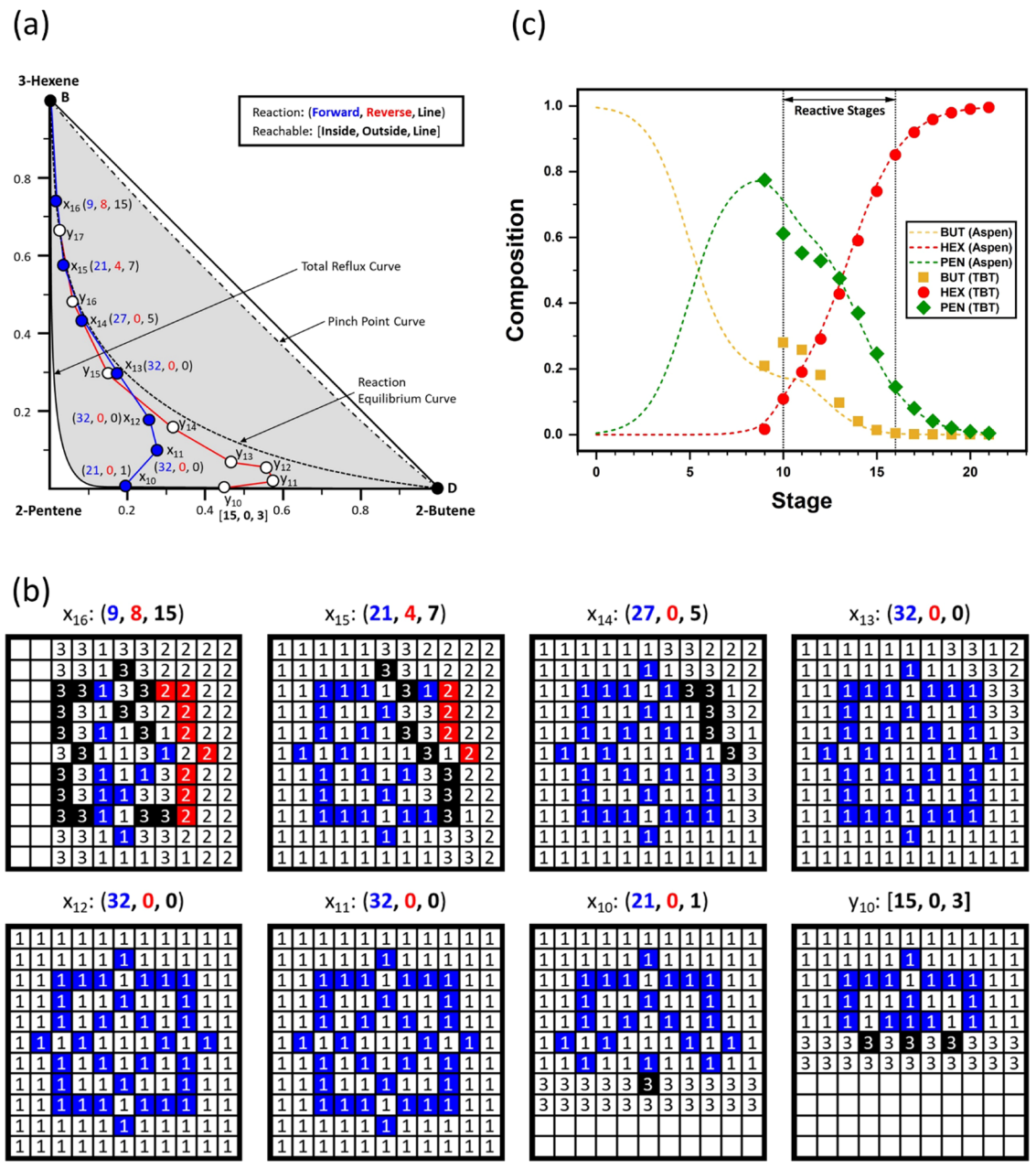

Figure 14. (a) Feasibility evaluation results of the RD column for the 2-pentene metathesis, (b) detailed results for the recognized edges of the liquid/vapor compositions of the 2-pentene metathesis RD column, and (c) comparison of the liquid composition profile between the rigorous simulation and tray-by-tray (TBT) calculations.

concluded that the RD column design is feasible, and this conclusion was further validated through a rigorous simulation.

Figure 14(c) compares the results between the stage calculations and the rigorous simulation, focusing on the liquid profile within the column. Detailed conditions of the RD column with the 2-pentene metathesis reaction for the rigorous simulation are provided in the Supporting Information (Section S7.2). The comparison shows a high degree of agreement between the calculated profiles and the rigorous simulation result. However, due to the cumulative errors in stage calculations initiated from the bottom composition (x_B), as the column moved up, the discrepancies in the composition profile of the reaction zone became more pronounced. Nevertheless, the overall profile shape remained similar, and the simulation result confirms that the designed RD column can produce 2-butene and 3-hexene with purities exceeding 99.5% at the top and bottom of the column, respectively.

4.3. Double-Feed Column: *tert*-Amyl Methyl Ether (TAME) Synthesis. The final case study focused on the feasibility evaluation of a double-feed RD column for the production of tert-amyl methyl ether (TAME). TAME is generated through a nonisomolar combination reaction, in which either 2-methyl-1-butene (2M1B) or 2-methyl-2-butene (2M2B) reacts with methanol (MeOH) at a 1:1 stoichiometric ratio.[57] We assumed that only a reaction between 2M1B and methanol occurs within the column in this case study. Since it is a nonisomolar reaction, it can be interpreted as having a finite reaction difference point. The feasibility evaluation was performed on a double-feed column, for which a portion of 2M1B is pre-reacted to form TAME and supplied as the lower

https://doi.org/10.1021/acsomega.3c08128
ACS Omega 2023, 8, 48413−48431

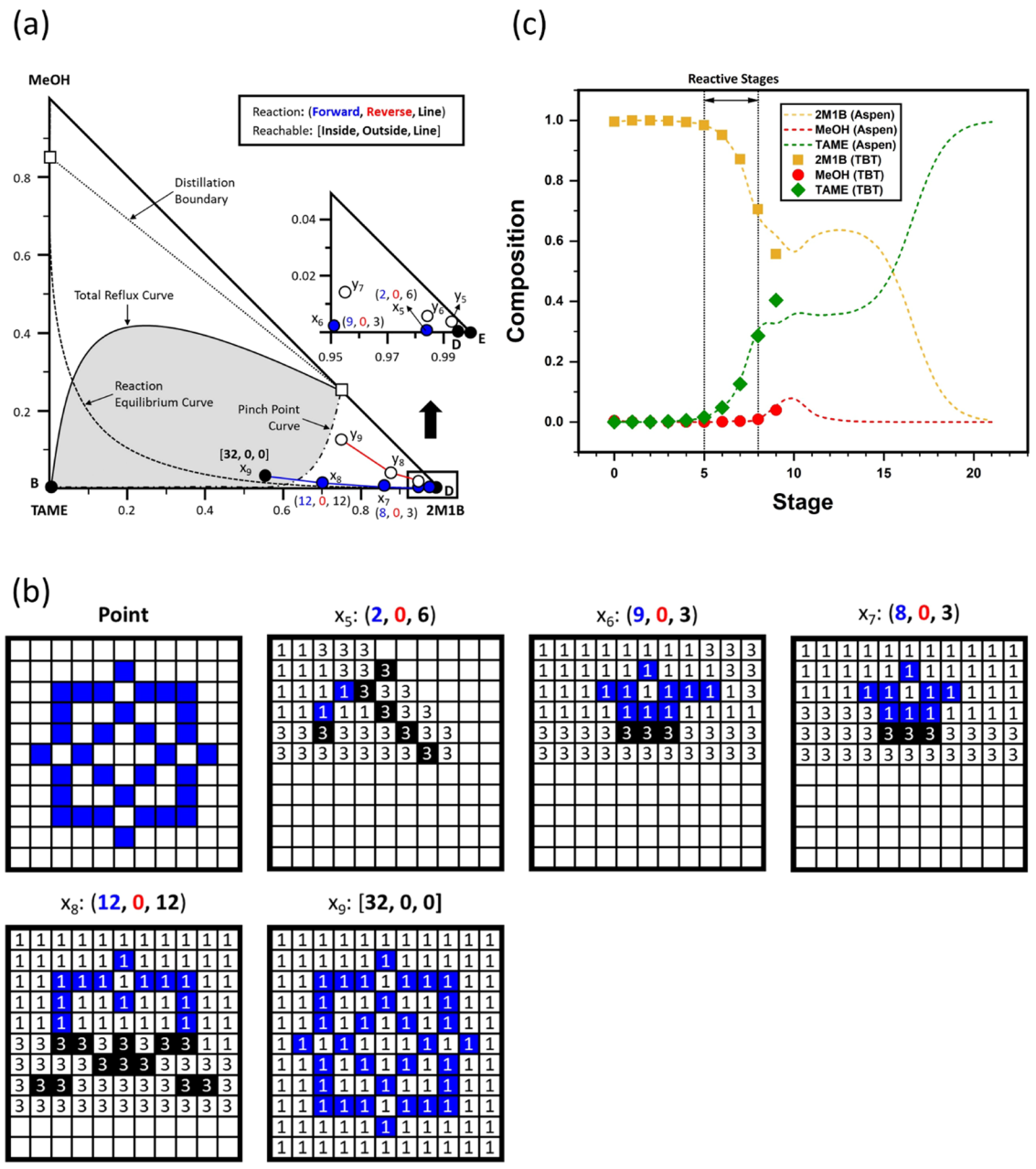

Figure 15. (a) Feasibility evaluation results of the RD column for the production of TAME, (b) detailed results for the recognized edges of the liquid compositions of the TAME synthesis RD column, and (c) comparison of the liquid composition profile between rigorous simulation and tray-by-tray (TBT) calculations.

feed while pure 2M1B is additionally supplied as the upper feed of the RD column. The RD column has a rectifying reaction zone, and it consists of four rectifying stages and four reactive stages.

Figure 15(a) represents the feasibility evaluation result of the double-feed column for the production of TAME. The liquid compositions of the reactive stages (5 to 8 stage) and liquid composition (x_9) passing through the reaction zone are presented. The evaluation reveals that all of the liquid compositions (x_5, x_6, x_7, x_8) of the reactive stages are located within the forward reaction zone, and the liquid composition (x_9) also falls within the reachable region. The detailed pixel recognition results for the TAME synthesis are listed in Figure 15(b). Therefore, the design of the double-feed column for the production of TAME is feasible.

Figure 15(c) compares the liquid composition profile obtained from the rigorous simulation and tray-by-tray calculations. The Supporting Information (Section S7.3) provides detailed conditions for rigorous simulation. Although a slight error is observed at the ninth stage, the variations in the results are insignificant and demonstrate a consistent trend. The rigorous simulation confirms that the RD design can produce TAME with a purity of over 99.5% at the bottom of the column.

Case studies were performed to assess the practical applicability of the proposed methodology: (1) a finite reaction difference point for the production of MTBE, (2) an infinite reaction difference point for 2-pentene metathesis, and (3) a double-feed column for TAME synthesis. In the case studies, since the proposed method relies on stage calculations,

https://doi.org/10.1021/acsomega.3c08128
ACS Omega 2023, 8, 48413−48431

an increase in the number of stages in an RD column led to an escalation of errors in the composition profile and additionally presented limitations in terms of evaluation time. However, the results of feasibility evaluations by the proposed automated method were validated through rigorous column simulations in Aspen Plus.

5. CONCLUSIONS

This study automated the feasibility evaluation procedure of RD columns using an AI-based region recognition approach to reduce the dependence on expert knowledge and heuristics in graphical methods. Using a machine learning-based computer vision algorithm, specifically the *k*-means clustering-based image segmentation method, the key topological information on the reaction and reachable regions was extracted from RCM images. Subsequently, the extracted information was used in stage calculations to perform automated feasibility evaluation of the RD columns. The proposed method was utilized to evaluate the feasibility of the RD columns with different types of reactions (nonisomolar combination/decomposition reaction and isomolar metathesis reaction) and feed types (single- and double-feed). The results were obtained within a few seconds, demonstrating the efficiency of the proposed approach. Furthermore, in the case studies, the feasibility evaluation results for the three examples were validated using rigorous simulation, confirming the effectiveness of the proposed method for actual industrial applications. Since the feasibility criteria proposed in previous studies serve as necessary conditions, they have limitations when applied to practical system designs. However, the method proposed in this study offers the advantage of automatically evaluating the feasibility within seconds using the simple information on the reaction equilibrium and phase equilibrium from various systems. Moreover, it can be applied not only to RD column design but also to the screening stage of various candidates for process intensification, and the method enables the expansion of its utility beyond system design.

■ ASSOCIATED CONTENT

Supporting Information

The Supporting Information is available free of charge at https://pubs.acs.org/doi/10.1021/acsomega.3c08128.

Reactive lever rules for RD columns (Figures S1−S4); detailed parameters of ternary mixtures; additional Aspen Plus simulation result (Figure S5); and Aspen Plus simulation environment and results for case studies (Figure S6) (PDF)

■ AUTHOR INFORMATION

Corresponding Author

Jae W. Lee − *Department of Chemical and Biomolecular Engineering, Korea Advanced Institute of Science and Technology (KAIST), Daejeon 34141, South Korea;* orcid.org/0000-0002-8756-0195; Email: jaewlee@kaist.ac.kr

Authors

Yongbeom Shin − *Department of Chemical and Biomolecular Engineering, Korea Advanced Institute of Science and Technology (KAIST), Daejeon 34141, South Korea*

Minyong Lee − *Department of Chemical and Biomolecular Engineering, Korea Advanced Institute of Science and Technology (KAIST), Daejeon 34141, South Korea*

Jeongwoo Lee − *Department of Chemical and Biomolecular Engineering, Korea Advanced Institute of Science and Technology (KAIST), Daejeon 34141, South Korea*

Donggun Kim − *Department of Chemical and Biomolecular Engineering, Korea Advanced Institute of Science and Technology (KAIST), Daejeon 34141, South Korea*

Complete contact information is available at: https://pubs.acs.org/10.1021/acsomega.3c08128

Notes

The authors declare no competing financial interest.

■ ACKNOWLEDGMENTS

This work was supported by the Engineering Research Center (ERC), funded by the National Research Foundation of Korea (NRF-2022R1A5A1033719), and Korea Environment Industry & Technology Institute (KEITI), funded by the Korean Ministry of Environment (MOE; 2022003490002).

■ REFERENCES

(1) Sholl, D. S.; Lively, R. P. Seven Chemical Separations to Change the World. *Nature* **2016**, *532* (7600), 435−437.

(2) Lucia, A.; McCallum, B. R. Energy Targeting and Minimum Energy Distillation Column Sequences. *Comput. Chem. Eng.* **2010**, *34* (6), 931−942.

(3) Kiss, A. A.; Smith, R. Rethinking Energy Use in Distillation Processes for a More Sustainable Chemical Industry. *Energy* **2020**, *203*, No. 117788.

(4) Kim, H. S.; Kim, Y.; Lim, H. S.; Kim, H.; Lee, J. W. Surface Enrichment of Lanthanum on Co3O4 for Stable Chemical Looping Combustion. *J. CO_2 Util.* **2023**, *73*, No. 102532.

(5) Stankiewicz, A.; Moulijn, J. A. Process Intensification. *Ind. Eng. Chem. Res.* **2002**, *41* (8), 1920−1924.

(6) Lee, H.; Mo, H.; Namgung, K.; Jang, W.; Lee, J. W. Energy-Efficient Design of a Novel Double Annular Separation Column Using Pinch Pressure. *Ind. Eng. Chem. Res.* **2020**, *59* (32), 14398−14409.

(7) Mtogo, J. W.; Toth, A. J.; Fozer, D.; Mizsey, P.; Szanyi, A. Effects of Energy Intensification of Pressure-Swing Distillation on Energy Consumption and Controllability. *ACS Omega* **2023**, *8* (1), 726−736.

(8) Harmsen, G. J. Industrial Best Practices of Conceptual Process Design. *Chem. Eng. Process.* **2004**, *43* (5), 671−675.

(9) Kaymak, D. B.; Ünlü, H.; Öfkeli, T. Control of a Reactive Distillation Column with Double Reactive Sections for Two-Stage Consecutive Reactions. *Chem. Eng. Process.* **2017**, *113*, 86−93.

(10) Lucia, A.; Amale, A.; Taylor, R. Energy Efficient Hybrid Separation Processes. *Ind. Eng. Chem. Res.* **2006**, *45* (25), 8319−8328.

(11) Siirola, J. J. Industrial Applications of Chemical Process Synthesis. *Adv. Chem. Eng.* **1996**, *23*, 1−62.

(12) Seo, C.; Lee, H.; Lee, M.; Lee, J. W. Temperature Driven Internal Heat Integration in an Energy-Efficient Partial Double Annular Column. *Korean J. Chem. Eng.* **2022**, *39* (2), 263−274.

(13) Malone, M. F.; Huss, R. S.; Doherty, M. F. Green Chemical Engineering Aspects of Reactive Distillation. *Environ. Sci. Technol.* **2003**, *37* (23), 5325−5329.

(14) Yang, A.; Lv, L.; Shen, W.; Dong, L.; Li, J.; Xiao, X. Optimal Design and Effective Control of the Tert-Amyl Methyl Ether Production Process Using an Integrated Reactive Dividing Wall and Pressure Swing Columns. *Ind. Eng. Chem. Res.* **2017**, *56* (49), 14565−14581.

(15) Gomez-Castro, F. I.; Rico-Ramirez, V.; Segovia-Hernandez, J. G.; Hernandez-Castro, S.; El-Halwagi, M. M. Simulation Study on Biodiesel Production by Reactive Distillation with Methanol at High

Pressure and Temperature: Impact on Costs and Pollutant Emissions. *Comput. Chem. Eng.* **2013**, *52*, 204−215.
(16) Jang, W.; Namgung, K.; Lee, H.; Mo, H.; Lee, J. W. Enhanced Energy Savings from Simultaneous Triple Esterification of C4 -C6 Alcohols in a Single Reactive Distillation Column. *Ind. Eng. Chem. Res.* **2020**, *59* (5), 1966−1978.
(17) Hu, Y.; Wang, L.; Lu, J.; Ding, L.; Zhang, G.; Zhang, Z.; Tang, J.; Cui, M.; Chen, X.; Qiao, X. Novel Reactive Distillation Process for Cyclohexyl Acetate Production: Design, Optimization, and Control. *ACS Omega* **2023**, *8* (14), 13192−13201.
(18) Chaniago, Y. D.; Hussain, A.; Andika, R.; Lee, M. Reactive Pressure-Swing Distillation toward Sustainable Process of Novel Continuous Ultra-High-Purity Electronic-Grade Propylene Glycol Monomethyl Ether Acetate Manufacture. *ACS Sustainable Chem. Eng.* **2019**, *7* (22), 18677−18689.
(19) Lee, H.; Jang, W.; Lee, J. W. Multiple Transesterifications in a Reactive Dividing Wall Column Integrated with a Heat Pump. *Korean J. Chem. Eng.* **2019**, *36* (6), 954−964.
(20) Lee, M.; Lee, H.; Seo, C.; Lee, J.; Lee, J. W. Enhanced Energy Efficiency and Reduced CO2 Emissions by Hybrid Heat Integration in Dimethyl Carbonate Production Systems. *Sep. Purif. Technol.* **2022**, *287*, No. 120598.
(21) Kim, D.; Lee, M.; Shin, Y.; Lee, J.; Lee, J. W. Direct Production of Diethyl Carbonate from Ethylene Carbonate and Ethanol by Energy-Efficient Intensification of Reaction and Separation. *Chem. Eng. Process.* **2023**, *192*, No. 109519.
(22) Al-Arfaj, M. A.; Luyben, W. L. Design and Control of an Olefin Metathesis Reactive Distillation Column. *Chem. Eng. Sci.* **2002**, *57* (5), 715−733.
(23) Malone, M. F.; Doherty, M. F. Reactive Distillation. *Ind. Eng. Chem. Res.* **2000**, *39* (11), 3953−3957.
(24) Taylor, R.; Miller, A.; Lucia, A. Geometry of Separation Boundaries: Systems with Reaction. *Ind. Eng. Chem. Res.* **2006**, *45* (8), 2777−2786.
(25) Almeida-Rivera, C. P.; Swinkels, P. L. J.; Grievink, J. Designing Reactive Distillation Processes: Present and Future. *Comput. Chem. Eng.* **2004**, *28* (10), 1997−2020.
(26) Lee, J. W.; Hauan, S.; Westerberg, A. W. Graphical Methods for Reaction Distribution in a Reactive Distillation Column. *AIChE J.* **2000**, *46* (6), 1218−1233.
(27) Lee, J. W.; Hauan, S.; Len, K. M.; Westerberg, A. W. A Graphical Method for Designing Reactive Distillation Columns I. the Ponchon-Savarit Method. *Proc. R. Soc. London, Ser. A* **2000**, *456* (2000), 1953−1964.
(28) Lee, J. W.; Hauan, S.; Lien, K. M.; Westerberg, A. W. A Graphical Method for Designing Reactive Distillation Columns II. the McCabe-Thiele Method. *Proc. R. Soc. London, Ser. A* **2000**, *456* (2000), 1965−1978.
(29) Lee, J. W.; Westerberg, A. W. Graphical Design Applied to MTBE and Methyl Acetate Reactive Distillation Processes. *AIChE J.* **2001**, *47* (6), 1333−1345.
(30) Lee, J. W.; Hauan, S.; Westerberg, A. W. Feasibility of a Reactive Distillation Column with Ternary Mixtures. *Ind. Eng. Chem. Res.* **2001**, *40* (12), 2714−2728.
(31) Lee, J. W. Feasibility Studies on Quaternary Reactive Distillation Systems. *Ind. Eng. Chem. Res.* **2002**, *41* (18), 4632−4642.
(32) Guo, Z.; Chin, J.; Lee, J. W. Feasibility of Continuous Reactive Distillation with Azeotropic Mixtures. *Ind. Eng. Chem. Res.* **2004**, *43* (14), 3758−3769.
(33) Kang, D.; Lee, K.; Lee, J. W. Feasibility Evaluation of Quinary Heterogeneous Reactive Extractive Distillation. *Ind. Eng. Chem. Res.* **2014**, *53* (31), 12387−12398.
(34) Guo, Z.; Ghufran, M.; Lee, J. W. Feasible Products in Batch Reactive Distillation. *AIChE J.* **2003**, *49* (12), 3161−3172.
(35) Kang, D.; Lee, J. W. Graphical Design of Integrated Reaction and Distillation in Dividing Wall Columns. *Ind. Eng. Chem. Res.* **2015**, *54* (12), 3175−3185.
(36) Chin, J.; Kattukaran, H. J.; Lee, J. W. Generalized Feasibility Evaluation of Equilibrated Quaternary Reactive Distillation Systems. *Ind. Eng. Chem. Res.* **2004**, *43* (22), 7092−7102.
(37) Chin, J.; Lee, J. W. Rapid Generation of Composition Profiles for Reactive and Extractive Cascades. *AIChE J.* **2005**, *51* (3), 922−930.
(38) Chin, J.; Lee, J. W.; Choe, J. Feasible Products in Complex Batch Reactive Distillation. *AIChE J.* **2006**, *52* (5), 1790−1805.
(39) Jantharasuk, A.; Gani, R.; Górak, A.; Assabumrungrat, S. Methodology for Design and Analysis of Reactive Distillation Involving Multielement Systems. *Chem. Eng. Res. Des.* **2011**, *89* (8), 1295−1307.
(40) Shah, M.; Kiss, A. A.; Zondervan, E.; De Haan, A. B. A Systematic Framework for the Feasibility and Technical Evaluation of Reactive Distillation Processes. *Chem. Eng. Process.* **2012**, *60*, 55−64.
(41) Li, P.; Huang, K.; Lin, Q. A Generalized Method for the Synthesis and Design of Reactive Distillation Columns. *Chem. Eng. Res. Des.* **2012**, *90* (2), 173−184.
(42) Li, H.; Meng, Y.; Li, X.; Gao, X. A Fixed Point Methodology for the Design of Reactive Distillation Columns. *Chem. Eng. Res. Des.* **2016**, *111*, 479−491.
(43) Pazmiño-Mayorga, I.; Jobson, M.; Kiss, A. A. Operating Windows for Early Evaluation of the Applicability of Advanced Reactive Distillation Technologies. *Chem. Eng. Res. Des.* **2023**, *189*, 485−499.
(44) Muthia, R.; Jobson, M.; Kiss, A. A. A Systematic Framework for Assessing the Applicability of Reactive Distillation for Quaternary Mixtures Using a Mapping Method. *Comput. Chem. Eng.* **2020**, *136*, No. 106804.
(45) Sasi, T.; Skiborowski, M. Automatic Synthesis of Distillation Processes for the Separation of Homogeneous Azeotropic Multicomponent Systems. *Ind. Eng. Chem. Res.* **2020**, *59* (47), 20816−20835.
(46) Dhanachandra, N.; Manglem, K.; Chanu, Y. J. Image Segmentation Using K -Means Clustering Algorithm and Subtractive Clustering Algorithm. *Procedia Comput. Sci.* **2015**, *54*, 764−771.
(47) Canny, J. A Computational Approach to Edge Detection. *IEEE Trans. Pattern Anal. Mach. Intell.* **1986**, *PAMI-8* (6), 679−698.
(48) Cheng, H. D.; Jiang, X. H.; Sun, Y.; Wang, J. Color Image Segmentation: Advances and Prospects. *Pattern Recognit.* **2001**, *34* (12), 2259−2281.
(49) Kanungo, T.; Mount, D. M.; Netanyahu, N. S.; Piatko, C. D.; Silverman, R.; Wu, A. Y. An Efficient K-Means Clustering Algorithms: Analysis and Implementation. *IEEE Trans. Pattern Anal. Mach. Intell.* **2002**, *24* (7), 881−892.
(50) Wahnschafft, O. M.; Koehler, J. W.; Blass, E.; Westerberg, A. W. The Product Composition Regions of Single-Feed Azeotropic Distillation Columns. *Ind. Eng. Chem. Res.* **1992**, *31* (10), 2345−2362.
(51) Wahnschafft, O. M.; Westerberg, A. W. The Product Composition Regions of Azeotropic Distillation Columns. 2. Separability in Two-Feed Columns and Entrainer Selection. *Ind. Eng. Chem. Res.* **1993**, *32* (6), 1108−1120.
(52) Lee, J. W.; Hauan, S.; Lien, K. M.; Westerberg, A. W. Difference Points in Extractive and Reactive Cascades. II — Generating Design Alternatives by the Lever Rule for Reactive Systems. *Chem. Eng. Sci.* **2000**, *55* (16), 3161−3174.
(53) Doherty, M. F.; Caldarola, G. A. Design and Synthesis of Homogeneous Azeotropic Distillations. 3. The Sequencing of Columns for Azeotropic and Extractive Distillations. *Ind. Eng. Chem. Fundam.* **1985**, *24* (4), 474−485.
(54) Matsuyama, H.; Nishimura, H. Topological and Thermodynamic Classification of Ternary Vapor-Liquid Equilibria. *J. Chem. Eng. Jpn.* **1977**, *10* (3), 181−187.
(55) Huang, K.; Wang, S. J.; Ding, W. Towards Further Internal Heat Integration in Design of Reactive Distillation Columns-Part III: Application to a MTBE Reactive Distillation Column. *Chem. Eng. Sci.* **2008**, *63* (8), 2119−2134.

https://doi.org/10.1021/acsomega.3c08128
ACS Omega 2023, 8, 48413−48431

(56) Okasinski, M. J.; Doherty, M. F. Design Method for Kinetically Controlled, Staged Reactive Distillation Columns. *Ind. Eng. Chem. Res.* **1998**, *37* (7), 2821−2834.
(57) Gao, X.; Wang, F.; Li, H.; Li, X. Heat-Integrated Reactive Distillation Process for TAME Synthesis. *Sep. Purif. Technol.* **2014**, *132*, 468−478.

https://doi.org/10.1021/acsomega.3c08128
ACS Omega 2023, 8, 48413−48431